

# Sensor Data Fusion in Top-View Grid Maps using Evidential Reasoning with Advanced Conflict Resolution

Sven Richter<sup>1,\*</sup>, Frank Bieder<sup>1,2</sup>, Sascha Wirges<sup>3</sup> and Christoph Stiller<sup>1,2</sup>

**Abstract**—We present a new method to combine evidential top-view grid maps estimated based on heterogeneous sensor sources. Dempster’s combination rule that is usually applied in this context provides undesired results with highly conflicting inputs. Therefore, we use more advanced evidential reasoning techniques and improve the conflict resolution by modeling the reliability of the evidence sources. We propose a data-driven reliability estimation to optimize the fusion quality using the Kitti-360 dataset. We apply the proposed method to the fusion of LiDAR and stereo camera data and evaluate the results qualitatively and quantitatively. The results demonstrate that our proposed method robustly combines measurements from heterogeneous sensors and successfully resolves sensor conflicts.

**Index Terms**—Autonomous driving, environment perception, sensor data fusion, evidential reasoning

## I. INTRODUCTION

For the navigation of automated vehicles, a detailed reconstruction of the environment is needed. In order to benefit from the individual strengths of different sensing principles, heterogeneous sensor setups are used. Top-view grid maps are especially suitable to model measurements from multimodal sensors and to combine them into one common representation. They enable modeling a wide range of information such as free space, the presence of obstacles and their semantic state and simplify information fusion due to their structured data format. Information fusion is particularly challenging, if contradicting information is combined. The combination rules that are frequently used for combining evidence measures in top-view grid maps such as Dempster’s or Yager’s rule perform unintuitively in those cases. We propose an adaptive method to handle this based on the ER framework presented by Yang *et al.* [1]. In case the sources provide conjunctive estimates, it reduces to Dempster’s rule. If the sources provide conflicting estimates, the combination is adapted based on a reliability coefficient assigned to each source of evidence individually. In this work, we combine evidential top-view grid maps estimated based on LiDAR and stereo camera measurements. The fusion

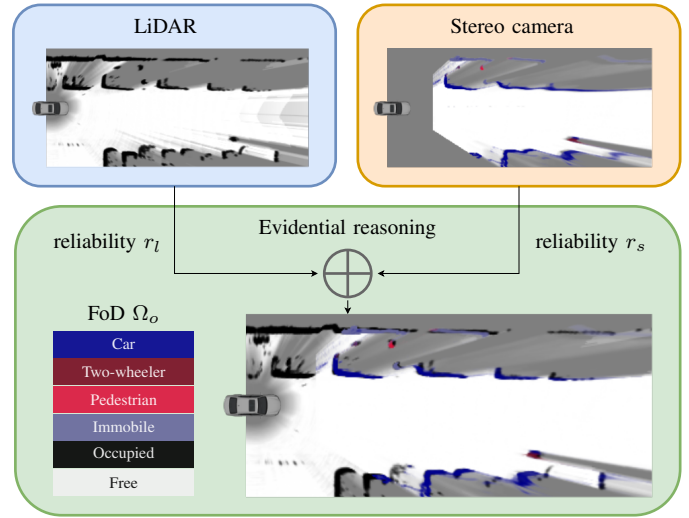


Fig. 1. The sensor data fusion framework presented in this work. Evidential grid maps modeling free space and semantic occupancy from LiDAR and stereo camera are combined with advanced conflict handling using sensor reliability coefficients  $r_l$  and  $r_s$ .

framework is sketched in Figure 1. The reliability coefficients  $r_l$  for the LiDAR and  $r_s$  for the stereo camera are estimated to optimize the fusion performance with respect to the ground truth bounding primitives in the Kitti-360 dataset [2].

## II. RELATED WORK

When combining degrees of evidence from independent sensor sources in grid maps, Dempster’s rule is usually applied [3], [4]. However, because of the above-mentioned shortcomings of this rule, other combination operators have been explored as well: Moras *et al.* [5] applied the partial conflict redistribution (PCR)<sup>6</sup> to the fusion of evidential occupancy grid maps. They tested their method with simulated LiDAR data that they fuse over time and showed an improved conflict resolution compared to Dempster’s rule. Li *et al.* [6] adapt the basic belief assignment (BBA) obtained from LiDAR and stereo cameras by adding a similarity factor and apply Dempster’s rule to the adapted BBAs. Compared to applying Dempster’s rule to the original BBAs, they obtain a reduced entropy and a higher specificity. Ullah *et al.* [7] proposed a new uncertainty measure based on Deng’s entropy and

<sup>1</sup> Authors are with the Institute of Measurement and Control Systems, Karlsruhe Institute of Technology (KIT), Karlsruhe, Germany. {sven.richter, frank.bieder, stiller}@kit.edu

<sup>2</sup> Authors are with the Mobile Perception Systems Group, FZI Research Center for Information Technology, Karlsruhe, Germany.

<sup>3</sup> Author is with the Bosch Center for Artificial Intelligence, Renningen, Germany. sascha.wirges@de.bosch.com

\* Corresponding author.

combine their entropy measures using Dempster's rule. By doing so, they could increase the accuracy of the fusion results compared to Dempster's rule and using Deng's original entropy.

The critical cases when fusing heterogeneous sensor data in top-view grid maps occur if the BBAs obtained from the individual sensors are highly conflicting similar to the example demonstrated in Tables I and II. We propose the inclusion of information on the credibility of the individual sensors in order to resolve those conflicts. This is not covered in the above-mentioned publications.

### III. EVIDENTIAL INFORMATION FUSION

Evidence Theory was formally introduced by Shafer in [8] and provides a framework to model uncertainty and combine evidence degrees from independent sources. Let  $\Omega$  be a set consisting of mutually excluding hypotheses of interest called frame of discernment (FoD) and  $2^\Omega$  its power set containing all subsets  $A \subseteq \Omega$ . The mapping

$$m: 2^\Omega \rightarrow [0, 1], \quad m(\emptyset) = 0, \quad \sum_{A \in 2^\Omega} m(A) = 1 \quad (1)$$

is called BBA and assigns a degree of evidence to all possible combinations of hypotheses. In order to derive a probability measure from a BBA, Smets proposed the pignistic transformation

$$\Pr(A) = \sum_{B \subseteq \Omega} \frac{|A \cap B|}{|B|} m(B) \quad (2)$$

in [9].

Analogously to Shannon's entropy measure for probabilistic random variables, it has been ongoing research to define similar measures in the evidence theoretical context. Deng's entropy

$$e_D(m) = - \sum_{A \subseteq \Omega} m(A) \log_2 \left( \frac{m(A)}{2^{|A|} - 1} \right), \quad (3)$$

presented in [10] can be written as the sum of the nonspecificity

$$ns_D(m) = \sum_{A \subseteq \Omega} m(A) \log_2 (2^{|A|} - 1) \quad (4)$$

and the discord

$$d_D(m) = - \sum_{A \subseteq \Omega} m(A) \log_2 (m(A)). \quad (5)$$

The nonspecificity  $ns_D(m)$  is a measure for the ignorance contained in the BBA and increases with BBA masses assigned to non singleton hypotheses. The discord  $d_D(m)$  is a measure for the indecision between several focal elements. The upper and lower bound of Deng's entropy are the BBA  $m_1$  assigning all the evidence mass  $m_1(\omega) = 1$  to one singleton hypothesis  $\omega \in \Omega$  and the distribution of total ignorance  $m_2(\Omega) = 1$ :

$$e_D(m_1) = 0 \leq ns_D(m) \leq \log_2 (2^{|\Omega|} - 1) = e_D(m_2) < |\Omega|. \quad (6)$$

In order to combine BBAs from independent sources, Dempster's rule of combination was introduced in [11]. Here, two BBAs  $m_1$  and  $m_2$  are combined as

$$(m_1 \oplus m_2)(A) = \frac{1}{1-K} \sum_{X \cap Y = A} m_1(X) m_2(Y), \quad (7)$$

where

$$K = \sum_{X \cap Y = \emptyset} m_1(X) m_2(Y) \quad (8)$$

denotes the accumulated conflict mass. The normalization constant  $\frac{1}{1-K}$  distributes the conflicts equally to all focal elements. Dempster's rule satisfies desired properties as commutativity and associativity. Although Dempster's rule is frequently used in literature, it has also been criticized. Zadeh showed in [12] that combining highly conflicting BBAs with Dempster's rule leads to counterintuitive results. This effect is also known as Zadeh's paradox. Table I shows such an example. Although both  $m_1$  and  $m_2$  hold high evidences masses against hypothesis  $B$ , Dempster's rule yields  $(m_1 \oplus m_2)(B) = 1$  ignoring the conflict mass  $K = 0.99$ .

TABLE I  
TWO BBAS  $m_1$  AND  $m_2$  ON  $\Omega = \{A, B, C\}$  COMBINED WITH  
DEMPSTER'S RULE (EQUATION (7)).

	A	B	C	$\Omega$
$m_1$	0.9	0.1	0	0
$m_2$	0	0.1	0.9	0
$m_1 \oplus m_2$	0	1	0	0

Different combination rules have been proposed aiming at resolving this counterintuitivity that all address different ways of dealing with conflicts. Yager [13] defined the conjunctive rule of combination given as

$$(m_1 \odot m_2)(A) = \sum_{X \cap Y = A} m_1(X) m_2(Y), \quad (9)$$

for  $A \neq \Omega$ , and

$$(m_1 \odot m_2)(A) = m_1(\Omega) m_2(\Omega) + \sum_{X \cap Y = \emptyset} m_1(X) m_2(Y) \quad (10)$$

for  $A = \Omega$ . Note that it merely drops the normalization constant and assigns the conflict mass  $K$  to  $\Omega$  compared to Dempster's rule in Equation (7). Table II shows the results

TABLE II  
TWO BBAS  $m_1$  AND  $m_2$  ON  $\Omega = \{A, B, C\}$  COMBINED WITH THE  
CONJUNCTIVE RULE (EQUATION (9)).

	A	B	C	$\Omega$
$m_1$	0.9	0.1	0	0
$m_2$	0	0.1	0.9	0
$m_1 \odot m_2$	0	0.01	0	0.99

when applying the conjunctive rule to the example introduced in Table I. Compared to Dempster's rule the conjunctive rule assigns the conflict mass  $K$  to  $(m_1 \odot m_2)(\Omega)$  indicating a high degree of uncertainty. Although the conjunctive rule gives a more intuitive result in this example it discards a significant

amount of information by assigning the whole conflict mass to  $\Omega$ . Other examples for modified combination rules are Duboi's and Prade's rule presented in [14] and the PCR rules introduced in [15], [16]. All of them are based on Yager's rule (Equation (9)) and assign conflict masses in different ways.

Yang *et al.* [1] propose another approach to dealing with conflicts when combining BBAs. Given the FoD  $\Omega$ , they consider sources of evidence  $\{e_i, i = 1, \dots, n\}$  with weight  $0 \leq w_i \leq 1$  and reliability  $0 \leq r_i \leq 1$  each providing a BBA  $m_i$ . The weight models the relative importance of the source of evidence, whereas the reliability models the information quality. The BBA  $m_i$  of the source of evidence  $e_i$  is modified based on the weight  $w_i$  and the reliability  $r_i$  as

$$\tilde{m}_i(A) = \begin{cases} 0, & \text{if } A = \emptyset, \\ \frac{1}{1+w_i-r_i} m_i(A), & \text{if } A \in \mathcal{P}(\Omega) \setminus \emptyset. \end{cases} \quad (11)$$

Two independent sources of evidence  $e_1$  and  $e_2$  with reliabilities  $0 \leq r_1, r_2 \leq 1$  and modified BBAs  $\tilde{m}_1$  and  $\tilde{m}_2$  are then combined as

$$m_{1,2}(A) = \begin{cases} 0, & \text{if } A = \emptyset, \\ \frac{\tilde{m}_{1,2}(A)}{\sum_{B \in \mathcal{P}(\Omega)} \tilde{m}_{1,2}(B)}, & \text{if } A \in \mathcal{P}(\Omega) \setminus \emptyset, \end{cases} \quad (12)$$

where

$$\begin{aligned} \tilde{m}_{1,2}(A) &= (1 - r_2) \tilde{m}_1(A) + (1 - r_1) \tilde{m}_2(A) \\ &+ \sum_{B \cap C = A} \tilde{m}_1(B) \tilde{m}_2(C). \end{aligned} \quad (13)$$

Note that for  $w_1 = w_2 = r_1 = r_2 = 1$ , Equation (12) reduces to Dempster's rule. In the remainder of this paper, Equation (12) will be referred to as evidential reasoning (ER) rule. The two reliability parameters  $r_1, r_2$  influence the combination results significantly. Table III shows the results

TABLE III  
TWO BBAs  $m_1$  AND  $m_2$  ON  $\Omega = \{A, B, C\}$  COMBINED WITH THE ER RULE (EQUATION (12)).

	A	B	C	$\Omega$
$m_1$ with $r_1 = 0.7$	0.9	0.1	0	0
$m_2$ with $r_2 = 0.3$	0	0.1	0.9	0
$m_1 \odot m_2$	0.67	0.11	0.22	0

when combining the two BBAs from Tables I and II with the ER combination rule where the reliabilities were set to  $r_1 = 0.7$  and  $r_2 = 0.3$  and  $w_1 = w_2 = 1$ . Due to the higher reliability assigned to  $m_1$ , the conflict between  $A$  and  $C$  is mostly assigned to  $A$ .

In summary, evidential reasoning with the ER combination rule (Equation (12)) provides a mathematical framework for dealing with differently credible sources of evidence without losing the mathematical properties of Dempster's original combination rule.

#### IV. METHODOLOGY

To the best of the author's knowledge the ER combination rule has not yet been applied to the fusion of evidential grid maps. Subsequently, we first present our evidential grid map

model and explain how the sensor grid maps are combined using ER.

##### A. Evidential Grid Map Model

In this work, we consider the semantic classes "car", "two-wheeler", "pedestrian", "other mobile obstacles" or "immobile obstacles". In particular, the occupancy FoD

$$\Omega_o := \{c, cy, p, m, nm, f, v\} \quad (14)$$

consists of the hypotheses displayed in Table IV. The BBA  $m$

TABLE IV  
THE FoD  $\Omega_o$  USED IN THE EVIDENTIAL GRID MAP REPRESENTATION. THE INDIVIDUAL SEMANTIC HYPOTHESES REFINE THE CLASSICAL OCCUPANCY HYPOTHESIS.

Semantic class	Set
Occupied by...	
... car	$\{c\}$
... two-wheeler	$\{cy\}$
... pedestrian	$\{p\}$
... other mobile object	$\{om\}$
... immobile object	$\{nm\}$
... unknown object type	$\{c, cy, p, om, nm\}$
Free	$\{f\}$

on  $2^{\Omega_o}$  is then represented by the multi-layer grid map

$$g: \mathcal{G} \times 2^{\Omega_o} \rightarrow [0, 1]. \quad (15)$$

Here, the two-dimensional (2D) Cartesian grid  $\mathcal{G} = \mathcal{P}_1 \times \mathcal{P}_2$  forms a partition of the rectangular region of interest  $\mathcal{R} = I_1 \times I_2 \subset \mathbb{R}^2$ , where

$$\begin{aligned} \mathcal{P}_i &= \{I_{i,k}, k \in \{0, \dots, s_i - 1\}\}, \\ I_{i,k} &= [o_i + k \delta_i, o_i + (k + 1) \delta_i), \quad i \in \{1, 2\}, \end{aligned}$$

with grid cell side length  $\delta_i \in \mathbb{R}$ , origin  $o_i \in \mathbb{R}$  and size  $s_i \in \mathbb{N}$ .

##### B. Evidential Reasoning with Reliability

We apply the ER combination rule presented by Yang *et al.* [1] to sensor grid maps and model the reliability  $r_i$  of sensor sources to improve conflict resolution. The importance weights  $w_i$  are set to one modeling all sources to be equally important. Given two sensor grid maps  $g_1$  and  $g_2$  calculated using measurements from two independent sensors  $s_1$  and  $s_2$ , the combination  $g_{1,2}$  is computed. The two sensors  $s_1$  and  $s_2$  are interpreted as sources of evidence with reliabilities  $0 \leq r_1, r_2 \leq 1$ . In a fixed grid cell  $C \in \mathcal{G}$ , the BBAs  $g_1(C, \cdot)$  and  $g_2(C, \cdot)$  are then combined to the BBA  $g_{1,2}(C, \cdot)$  using the ER rule.

The reliability of a source of evidence should be chosen carefully. Let  $m_1$  and  $m_2$  be two BBAs to be combined. We propose to model the reliabilities  $r_i$  as a function of the conflict mass

$$K = \sum_{X \cap Y = \emptyset} m_1(X) m_2(Y) \quad (16)$$

and the credibility coefficient  $b_i$  as

$$r_i = f_r(K, b_i) = 1 - (1 - b_i) K. \quad (17)$$

The coefficient  $0 \leq b_i \leq 1$  models the credibility of a source of evidence in light of a conflict. If  $K = 0$ , then  $r_1 = r_2 = 1$  and the ER rule reduces to Dempster’s rule. The higher the conflict mass  $K$ , the more unintuitive the combination result with Dempster’s rule becomes as shown in Table I and the combination rule is adapted. If  $K = 1$ , we have  $r_i = b_i$  and the credibility coefficient fully serves as reliability value.

In this work we apply the presented general framework to the combination of grid maps estimated based on one LiDAR scanner and one stereo camera each representing the BBA on the FoD  $\Omega_o$ .

### C. Parameter Estimation

When combining LiDAR and stereo camera sensor grid maps with the ER rule, the sensor credibility coefficients  $b_l$  for the LiDAR and  $b_s$  for the stereo camera need to be specified. In this work, we propose a data-driven approach assigning the values  $b_l, b_s$  resulting in the best fusion performance in terms of a quantitative evaluation. We use the three-dimensional (3D) semantic bounding primitives and the semantic point cloud in the Kitti-360 dataset to generate a reference semantic evidential grid map  $g_{\text{ref}}$ . Kitti-360 accumulates LiDAR measurement chunks containing over 300 frames. Each frame includes LiDAR reflections with a distance of at most 30m. The accumulated point clouds were semantically annotated and used to fit bounding primitives representing object instances and infrastructural entities such as buildings, poles and streets. The labeled bounding primitives and the accumulated point clouds are projected into the reference grid map  $g_{\text{ref}}$  representing the reference BBA per grid cell. As a quality measure, we define the evidential intersection over union (eIoU)

$$\text{eIoU}_\omega = \frac{\text{eTP}_\omega}{\text{eTP}_\omega + \text{eFP}_\omega + \text{eFN}_\omega} \quad (18)$$

based on the evidential true positive rate

$$\text{eTP}_\omega = \sum_{C \in \mathcal{G}_{xy}} \sum_{\phi \cap \omega = \phi} g_{\text{ref}}(C, \phi) g_{\mathcal{M}}(C, \omega), \quad (19)$$

the false positive rate

$$\text{eFP}_\omega = \sum_{C \in \mathcal{G}_{xy}} \sum_{\phi \cap \omega = \emptyset} g_{\text{ref}}(C, \phi) g_{\mathcal{M}}(C, \omega), \quad (20)$$

and false negative rate

$$\text{eFN}_\omega = \sum_{C \in \mathcal{G}_{xy}} \sum_{\phi \cap \omega = \emptyset} g_{\text{ref}}(C, \omega) g_{\mathcal{M}}(C, \phi). \quad (21)$$

Note that the eIoU reduces to the classical intersection over union (IoU) used for pixel-wise semantic labeling if the BBA is binary, i.e.  $m(\omega) = 1$  for one  $\omega \in 2^\Omega$ .

Now, the performance of the information fusion is quantified by the eIoU (Equation (18)) for the hypotheses *occupied by unknown object type*. More specificity, we apply the ER rule to LiDAR and stereo camera sensor grid maps based on measurements in the Kitti-360 dataset [2] for credibility values

$$\{(b_l, b_s) \mid b_l, b_s \in 0.1 \cdot \mathbb{N}_{\leq 10}\}.$$

$b_l \backslash b_s$	0.0	0.1	0.2	0.3	0.4	0.5	0.6	0.7	0.8	0.9	1.0
0.0	91.75	91.65	91.54	91.43	91.31	91.19	91.06	90.93	90.8	90.67	90.54
0.1	91.9	91.8	91.69	91.58	91.46	91.33	91.2	91.06	90.93	90.79	90.65
0.2	92.05	91.95	91.85	91.73	91.61	91.49	91.35	91.21	91.06	90.91	90.76
0.3	92.21	92.11	92.01	91.9	91.78	91.65	91.52	91.37	91.21	91.05	90.89
0.4	92.37	92.28	92.19	92.08	91.97	91.84	91.7	91.55	91.38	91.21	91.03
0.5	92.54	92.46	92.37	92.27	92.16	92.04	91.9	91.75	91.58	91.39	91.19
0.6	92.72	92.65	92.57	92.48	92.37	92.26	92.12	91.97	91.8	91.6	91.37
0.7	92.9	92.84	92.77	92.69	92.6	92.5	92.37	92.23	92.05	91.84	91.58
0.8	93.08	93.03	92.98	92.92	92.84	92.76	92.65	92.52	92.36	92.14	91.84
0.9	93.26	93.23	93.19	93.15	93.1	93.04	92.96	92.87	92.74	92.55	92.18
1.0	93.44	93.42	93.4	93.38	93.36	93.33	93.31	93.27	93.23	93.18	93.03

Fig. 2. The eIoUs of the hypotheses *occupied by unknown object type* for different combinations of credibility coefficients  $(b_l, b_s)$ . The highest eIoU is achieved for  $b_l = 1$  and  $b_s = 0$ .

In this context, all the occupancy evidence is assigned to the hypothesis *occupied by unknown object type* as the individual semantic hypotheses are not considered in the analysis. The results are shown in the table in Figure 2. Each entry contains the eIoU averaged over all cell states in 50 frames of the Kitti-360 dataset. It can be seen that the eIoU increases with increasing LiDAR credibility  $b_l$ , independent of the stereo camera credibility. Furthermore, the eIoUs increases for decreasing stereo camera credibilities. The highest eIoU is measured for the LiDAR credibility  $b_l = 1$  and the stereo camera credibility  $b_s = 0$ . For this combination of credibility values, the eIoU is 0.41 percentage points higher compared to applying Dempster’s rule and 2.9 percentage points higher than with  $b_l = b_s = 0$ . This difference is quite significant considering that the sensor estimates are not conflicting in the majority of the grid cells and both rules coincide in those cases. Recall that  $b_s = 0$  does not mean that the BBA estimated with the stereo camera is not regarded at all in the combination. It merely means that in cases where the stereo camera provides a measurement that disagrees with the LiDAR measurement, the LiDAR measurement shall be considered more reliable. The eIoU-based analysis shows how close the fusion result is to the reference grid map based on the semantic labels and bounding box primitives in the Kitti-360 dataset. As those labels were annotated using the LiDAR measurements this result does not really come as a surprise. However, this demonstrates that the sensor fusion results can be tuned as desired by adapting the credibility coefficients in the ER rule. As we consider the annotations in the Kitti-360 dataset to be accurate in this work, we therefore set  $b_l = 1$  and  $b_s = 0$  for the remainder of this paper. This is sensible as in fact, LiDAR scanners provide more accurate depth estimates compared to the disparity-based depth estimation with stereo cameras.

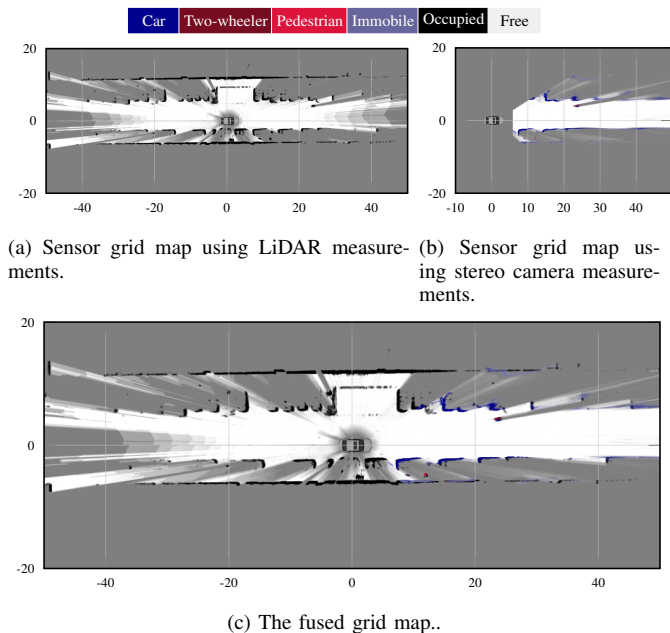


Fig. 3. Resulting evidential grid map for the fusion of LiDAR measurements without and stereo camera measurements with semantic estimates using the ER rule.

## V. EXPERIMENTS

We evaluate the fusion results qualitatively and quantitatively based on Velodyne HDL-64E LiDAR and stereo camera measurements in the Kitti-360 dataset presented in [2].

### A. Qualitative Results

We show qualitative results for the fusion of sensor grid maps from Velodyne HDL-64E LiDAR scans without semantic estimates with sensor grid maps from disparity maps from stereo images with semantic estimates.

Figure 3 shows the grid maps for one frame. In the sensor grid map based on LiDAR measurements that is depicted in Figure 3a, BBA estimates are only available for the hypotheses *free* and *occupied by unknown object type*. The grid map based on stereo camera measurements depicted in Figure 3b contains BBA estimates for the individual semantic hypotheses based on the semantic labeling provided by the neural network. Both sensor grid maps are estimated using the method described in [17] where the stereo camera grid map is based on stereo disparities obtained from the guided aggregation net for stereo matching presented by Zhang *et al.* [18] and the pixel-wise semantic labels are estimated using the network presented by Zhu *et al.* [19]. It can be seen that the spatial uncertainty is higher in the stereo camera grid map indicated by a more blurry occupancy pattern. The result of combining the two sensor grid maps with the ER rule is shown in Figure 3c. The semantic estimates provided by the stereo camera is successfully included in the occupancy pattern obtained from the LiDAR scanner.

In order to demonstrate the effect of using different evidential combination rules in case of conflicting sensor BBAs, the same sensor grid maps are combined using Dempster’s

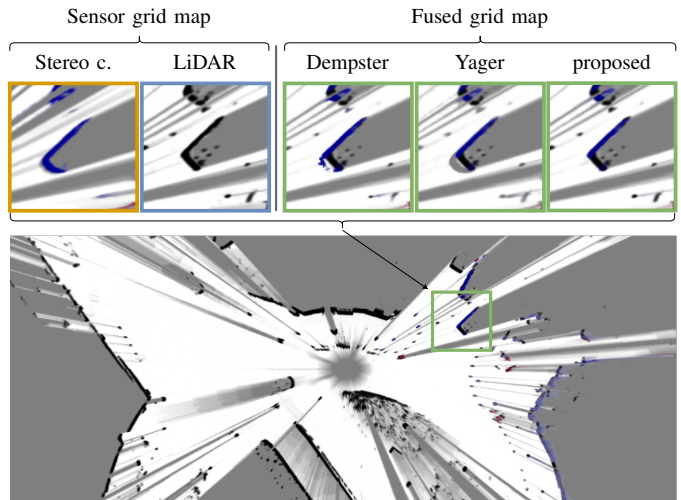


Fig. 4. Results for fusing LiDAR grid maps with stereo camera grid maps using different combination rules. A subarea is highlighted where a vehicle is located. The measurement conflict between the BBAs provided by the two sensors is resolved differently. Only the proposed method resolves the conflict correctly in most of the grid cells.

rule (Equation (7)), Yager’s rule (Equation (9)) and the ER rule (Equation (12)) in Figure 4. In this example, the distance of an observed car was underestimated by the stereo pipeline leading to an occupied-free conflict in front of the car. With Dempster’s rule, conflicting BBAs are distributed equally over all focal elements. Hence, large parts of the conflict mass are assigned to the hypothesis car. Yager’s rule assigns all conflict masses to  $\Omega$ , thus leading to a low BBA for both hypotheses free and car. The ER rule on the other hand is able to correctly assign large parts of the conflict masses to the hypothesis free due to the lower credibility coefficient  $r_s$  assigned to the stereo camera.

### B. Quantitative Evaluation

We evaluate the accuracy of the BBA by calculating the eIoU in 3000 frames of the Kitti-360 dataset for the fused grid maps and comparing it to the results obtained for the sensor measurement grid maps. The hypotheses *occupied by immobile object* and *occupied by other mobile object* are not considered here as the reference BBA for the former was found to be not credible, and the latter is barely observed in the evaluation dataset.

Figure 5 shows the results for the FoD  $\Omega_o$  in the described sensor setup. Because no semantic estimates are included in the LiDAR-based estimation chain, the eIoU values are zero for all semantic occupancy hypotheses. As expected, it can be seen that the LiDAR scanner leads to a more accurate BBA estimation than the stereo camera for the hypotheses estimated by both sensors. Furthermore, the metrics show that the accuracy for the singleton hypotheses *car*, *two-wheeler* and *pedestrian* can be significantly improved by fusing the occupancy semantics estimation obtained from the stereo camera with the occupancy information obtained from the LiDAR. Although no further semantic estimates are added in

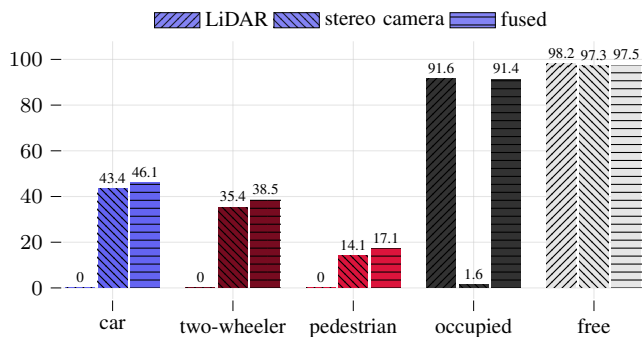


Fig. 5. The eIoUs in % for five hypotheses in the FoD  $\Omega_o$ . For each hypothesis, the bar plots show the eIoUs measured in the grid map based on LiDAR measurements, stereo camera measurements and for the fused grid map. The BBA from the stereo camera contains estimates for the semantic occupancy hypotheses whereas the LiDAR-based BBA only contains evidence for the hypotheses *occupied by unknown object type* and *free*.

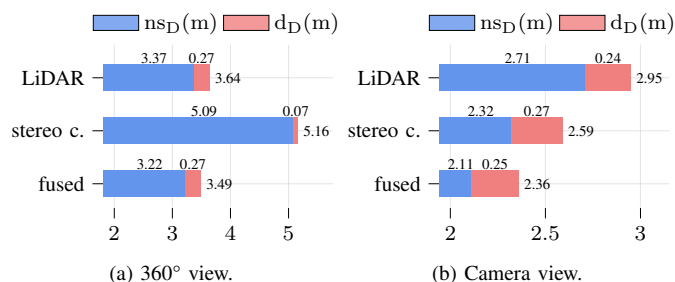


Fig. 6. Nonspecificity  $ns_D$  (m) and discord  $d_D$  (m) for LiDAR, stereo camera and fused grid maps.

the fusion process the eIoU can be improved by 6.2% for *cars*, by 8.8% for *two-wheelers* and by 21.3% for *pedestrians*. This is due to the improved conflict resolution when applying the ER combination rule as verified in Figure 4.

In addition to the comparison with reference BBA maps, the uncertainty incorporated in the estimated BBA is evaluated based on Deng’s entropy measures defined in Equations (3) to (5). Figure 6 shows Deng’s nonspecificity, discord and entropy averaged over the same 3000 frames of the Kitti-360 dataset for LiDAR, stereo camera and fused measurements. For each grid map, either all grid cells within a distance of 30 m to the ego vehicle (360° view) or the grid cells that are additionally within the viewing area of the stereo camera (camera view), respectively, are taken into account. In the 360° view shown in Figure 6a, we observe that the average entropy is highest in the stereo camera grid maps. This is expected as the stereo camera does not provide measurements outside the stereo camera view. After applying the proposed sensor data fusion, the entropy is reduced by 4.1% compared to the LiDAR grid map. The competitive part of the sensor data fusion is evaluated in the overlapping viewing areas of the sensors. The corresponding entropy measures are plotted in Figure 6b. Here, the entropy in the LiDAR grid map is higher than the entropy in the stereo camera. Again the best result is obtained after applying the proposed sensor data fusion. Due to a significant reduction of the nonspecificity, the entropy in

the fused grid map is reduced by 8.9% compared to the stereo camera grid map. This demonstrates that the introduced fusion operator successfully aggregates information from different sources while keeping the discord at a constant level.

## VI. CONCLUSION

We proposed to apply evidential reasoning (ER) to sensor data fusion in top-view grid maps. By resolving sensor conflicts adaptively based on reliability coefficients, we achieved accurate and robust fusion results even for highly conflicting sensor measurements. The reliabilities for one LiDAR scanner and one stereo camera were estimated by comparing the fusion results for different values and choosing the ones providing the best performance. We demonstrated the advantages of our approach compared to traditional combination rules such as the one’s by Dempster and Yager based on real sensor data. Future work will focus on combining the fused evidential grid maps from different time points in a recursive estimator to accumulated measurements over time and infer the dynamic state.

## REFERENCES

- [1] J.-B. Yang and D.-L. Xu, “Evidential reasoning rule for evidence combination,” *Artificial Intelligence*, vol. 205, pp. 1–29, 2013, ISSN: 0004-3702.
- [2] Y. Liao, J. Xie, and A. Geiger, “KITTI-360: A novel dataset and benchmarks for urban scene understanding in 2d and 3d,” *arXiv.org*, vol. 2109.13410, 2021.
- [3] D. Nuss, M. Thom, A. Danzer, and K. Dietmayer, “Fusion of laser and monocular camera data in object grid maps for vehicle environment perception,” in *17th International Conference on Information Fusion (FUSION)*, 2014, pp. 1–8.
- [4] G. Tanzmeister and D. Wollherr, “Evidential grid-based tracking and mapping,” *IEEE Transactions on Intelligent Transportation Systems*, vol. 18, no. 6, pp. 1454–1467, 2017.
- [5] J. Moras, J. Dezert, and B. Pannetier, “Grid occupancy estimation for environment perception based on belief functions and pcr6,” vol. 9474, Apr. 2015.
- [6] J. Li, H. Li, and H. Zeng, “Segm: A novel semantic evidential grid map by fusing multiple sensors,” in *Pattern Recognition and Computer Vision: Third Chinese Conference, PRCV 2020, Nanjing, China, October 16–18, 2020, Proceedings, Part I*, Nanjing, China: Springer-Verlag, 2020, pp. 155–166, ISBN: 978-3-030-60632-9.
- [7] I. Ullah, J. Youn, and Y.-H. Han, “Multisensor data fusion based on modified belief entropy in dempster-shafer theory for smart environment,” *IEEE Access*, vol. 9, pp. 37 813–37 822, 2021.
- [8] G. Shafer, “A mathematical theory of evidence,” 1976.
- [9] P. Smets, “The combination of evidence in the transferable belief model,” *IEEE Transactions on Pattern Analysis and Machine Intelligence*, vol. 12, no. 5, pp. 447–458, 1990.
- [10] Y. Deng, “Deng entropy,” *Chaos, Solitons & Fractals*, vol. 91, pp. 549–553, 2016, ISSN: 0960-0779.
- [11] A. P. Dempster, “Upper and Lower Probabilities Induced by a Multivalued Mapping,” *The Annals of Mathematical Statistics*, vol. 38, no. 2, pp. 325–339, 1967.
- [12] L. Zadeh, “On the validity of dempster’s rule of combination of evidence,” EECS Department, University of California, Berkeley, Tech. Rep. UCB/ERL M79/24, Mar. 1979.
- [13] R. R. Yager, “On the dempster-shafer framework and new combination rules,” *Information Sciences*, vol. 41, no. 2, pp. 93–137, 1987, ISSN: 0020-0255.

- [14] D. Dubois and H. Prade, "Representation and combination of uncertainty with belief functions and possibility measures," *Computational Intelligence*, vol. 4, no. 3, pp. 244–264, 1988. eprint: <https://onlinelibrary.wiley.com/doi/pdf/10.1111/j.1467-8640.1988.tb00279.x>.
- [15] F. Smarandache and J. Dezert, "Proportional conflict redistribution rules for information fusion," *Advances and Applications of DSMT for Information Fusion (Collected Works)*, vol. 2, pp. 3–68, 2006, Cited By :89.
- [16] F. Smarandache and J. Dezert, *Advances and Applications of DSMT for Information Fusion*. Jan. 2006.
- [17] S. Richter, F. Bieder, S. Wirges, and C. Stiller, *Mapping lidar and camera measurements in a dual top-view grid representation tailored for automated vehicles*, 2022.
- [18] F. Zhang, V. Prisacariu, R. Yang, and P. H. S. Torr, "Ga-net: Guided aggregation net for end-to-end stereo matching," in *2019 IEEE/CVF Conference on Computer Vision and Pattern Recognition (CVPR)*, 2019, pp. 185–194.
- [19] Y. Zhu, K. Sapra, F. A. Reda, K. J. Shih, S. Newsam, A. Tao, *et al.*, "Improving semantic segmentation via video propagation and label relaxation," in *Proceedings of the IEEE Conference on Computer Vision and Pattern Recognition*, 2019, pp. 8856–8865.